MACROSEGREGATION DURING PLANE FRONT DIRECTIONAL SOLIDIFICATION OF CsI-1 wt% TlI ALLOY

I.M.S. Sidawi# and S.N. Tewari*[1]

ABSTRACT

Macrosegregation produced during vertical Bridgman directional solidification of CsI-1 wt% TlI in crucibles of varying diameter, from 0.5 to 2.0 cm, has been examined. Gravity driven convection is present in the melt even in the smallest crucible diameter of 0.5 cm. Observed solutal profiles are in agreement with the analytical boundary layer model of Favier which describes macrosegregation in the presence of convection. The scintillation efficiency of CsI decreases along the specimen length as the thallium iodide content of the alloy increases.

INTRODUCTION

Because of the improved yield and quality crystal growers would ideally like to produce directionally solidified single crystals with a uniform distribution of solute (dopant) both along the length (axial) and across the diameter (radial). The Bridgman-Stockbarger technique of crystal growth where an alloy melt is directionally solidified by withdrawing the crucible at a constant speed (R) while a constant thermal gradient (G_l) is imposed at the liquid-solid interface, is used extensively in growing electronic materials. In the absence of convection the growing solid is expected (Refs. 1-2) to show an initial transient with continuously increasing solute content (for alloys with solutal partition coefficient, k<1). The initial solute build up in the melt at the liquid-

[1] #Graduate Student, Mechanical Engineering Department and *Professor, Chemical Engineering Department Cleveland State University, Cleveland, OH 44115.

solid interface stops when the rate of solute rejection becomes equal to the rate of transport by diffusion into the melt. Further steady-state growth produces a solid with a constant solute content (equal to the initial alloy composition, C_o). Because of the impingement of the solutal boundary layer with the last portion to solidify a final transient of sharp solutal build up occurs near the end of the solidification.

Fluid flow can result from destabilizing thermal profiles (density gradients in the melt transverse to the gravity vector) even during directional solidification with a positive thermal gradient in the melt at the liquid-solid interface. Such radial thermal gradients are virtually impossible to eliminate because of the mismatch in the thermal properties of the solid, liquid and the crucible materials at the interface near the wall (Refs. 3,4). These radial gradients may initiate natural convection even in alloys where the solute enrichment results in increased melt density.

Convection enhances the solute transport into the melt and influences the axial and radial dopant distributions. Numerical (Refs. 5,6) and analytical (Refs. 7-10) models have been presented in the literature to predict the influence of convection on the dopant distribution. Burton, Prim and Slichter (Ref. 7) visualized the development of a momentum boundary layer thickness (δ) inside which the solute was transported by diffusion. The rest of the melt, beyond the distance δ from the interface, was mixed and had a uniform composition. For $\delta << (D_l/R)$ they predicted the resulting axial solutal profile in terms of an effective partition coefficient ($k_e = k/(k+(1-k)\exp(-\delta R/D_l))$, where R is the growth speed and, D_l, the solutal diffusivity in the melt). Using a similar approach Favier (Refs. 8,9) analyzed the dopant distribution during Bridgman growth in the presence of convection. However, unlike the previous analyses which were

valid only for the two extremes, pure diffusion [$\delta >> (D_l/R)$] or extensive convection [$\delta << (D_l/R)$], he was able to predict the behavior for the whole range of $\Delta = \delta R/D_l$ values. This analysis showed a good agreement with the more accurate analytical solutions at both the extremes; for $\delta >> (D_l/R)$ it agrees with Burton, Prim and Slichter (Ref. 7) and for $\delta << (D_l/R)$ it agrees with Tiller, Jackson, Rutter and Chalmers (Ref. 2).

The axial and radial macrosegregations during Bridgman growth of binary alloys have been extensively investigated. However, there is no study where the actual fluid flow and the liquid-solid interface have been observed during crystal growth and correlated with the resulting solutal profiles. The purpose of this study was to observe the natural convection and examine its influence on the resulting dopant distribution during plane front solidification of CsI-1 wt% TlI. The CsI-TlI system was selected because the liquid is transparent to visual light, it can be directionally solidified in transparent quartz ampoules and the alloy has a simple phase diagram with large solubility and a reasonable partition coefficient, about 0.3 (Ref. 11). Thallium doped cesium iodide is also an important commercial scintillator material used mainly for gamma ray detection (Refs. 12-14). Its scintillation efficiency (light output) is expected to depend on the dopant distribution. However, despite its commercial importance the dependence of its scintillation efficiency on TlI content has not been systematically investigated (Ref. 13).

EXPERIMENTAL

ALLOY PREPARATION AND DIRECTIONAL SOLIDIFICATION: Typically about a 30 gram charge of cesium-iodide (99.99% purity) and thallium-iodide (99.99% purity) obtained from Anderson's Physics Laboratories was transferred into a quartz tube

inside a dry glove box. The charge was vacuum encapsulated after degassing for 60 minutes (10^{-3} Torr, 770 K). It was melted, mechanically mixed and rapidly quenched by pouring water on the quartz outer walls. The solid thus obtained was then crushed inside the dry glove box to provide material for subsequent directional solidification or phase diagram determination. The CsI-1wt%TlI alloy prepared in the above manner was vacuum encapsulated in cylindrical ampoules (0.5 cm, 1 cm and 2 cm diameter, 20 cm long) for directional solidification. Length of the initial melt column were respectively 10.4 cm, 8.2 cm and 6.9 cm for 0.5 cm, 1 cm and 2 cm ID ampoules.

Fig. 1 shows a schematic view of the directional solidification furnace. The resistance heated transparent quartz furnace is composed of four separate uniformly wound heating zones (each 12.7 cm long and 3.8 cm ID), whose temperatures can be separately programmed and controlled. The nickel-chromium alloy heating elements (1.0 mm diameter wire) are located in the gap between two coaxial quartz tubes, as shown in Fig. 1. The cylindrical quartz ampoules containing the charge are supported by a fine nichrome wire. The ampoule can be translated by the help of a stepping motor at speeds from 0.01 to 50 μms^{-1}. Some of the ampoules had a capillary quartz well ($\approx$0.5mm ID) into which fine refractory coated chromel-alumel thermocouples (0.05 mm diameter) were inserted to measure the temperature inside the solidifying specimen. Temperatures close to the outer surface of the ampoules were also recorded at several locations along their length. The liquid-solid interface location and shape were observed and recorded by the help of a video camera. Any change in the interface location was observed with respect to one of the stationary heating coils in the view. The four heating zones were first brought up to the predetermined

temperatures to melt the charge completely. The ampoules were then lowered at 0.4 $\mu m\ s^{-1}$ through a thermal gradient (G_l) of 34 K cm^{-1} in the melt at the liquid-solid interface to obtain the directionally solidified material.

MACROSEGREGATION AND SCINTILLATION EFFICIENCY: Thin slices (about 2-4 mm wide) cut along the length of the directionally solidified specimens were analyzed by atomic absorption spectroscopy to obtain the distribution of thallium. Some of these slices (for 1 and 2 cm diameter samples) were mounted and metallographically polished for examining the radial macrosegregation by electron microprobe. Very low intensity electron beams (15 kva, 0.05 μa) were used for the microprobe analysis to avoid charging and damage to the CsI crystals. The transverse slices from the 2 cm diameter specimen were initially used for the light output measurement before being destroyed for the subsequent atomic absorption analysis.

Fig. 2 shows a schematic view of the apparatus for measuring the scintillation efficiency (light output) of the alloy specimens. A collimated beam of 60 kev gamma line (corresponds to an absorption distance of about 0.2 cm in CsI) produced from an Am^{241} source impinged on the crystal. The light intensity recorded by the photomultiplier kept within the dark box was amplified and recorded on a multichannel spectrum analyzer. This technique allows a spatial resolution of about 0.3cm.

PHASE DIAGRAM: Since the CsI-TlI phase diagram is not accurately known for low thallium iodide content, a Perkin Elmer differential scanning calorimeter (DSC) was used to obtain the phase diagram for TlI content up to 2.5 wt%. Typically five to six specimens were examined for each alloy composition to obtain the solidus (corresponding to the average of the onset of melting during heating, Th_1, and the end

of solidification during cooling, Tc_2) and liquidus (corresponding to the average of the onset of solidification during cooling, Tc_1, and the end of melting during heating, Th_2) temperatures from the DSC output.

RESULTS

The experimentally observed CsI-TlI phase diagram for the low solute contents of our interest is shown in Fig. 3. Circles denote the liquidus and diamonds denote the solidus temperatures. Typical scatter, about 5 K, is shown in this figure for only one datum for the sake of clarity in the presentation. The solidus and liquidus lines approximately represent an average behavior through the data points. A range of melting points, 899 to 903 K, have been reported for pure CsI in the literature (Refs. 11,15). Our measurements indicated this temperature to be 903 K. The solute partition coefficient varies from 0.1 to 0.12 with the increasing thallium iodide content up to about 1.5 wt%. These values are much smaller than $k \approx 0.3$, which would have been estimated by extending the literature reported (Ref. 11) liquidus and solidus lines for the significantly larger solute contents, 11 mole% CsI. We will use a k value of 0.12 for analyzing our macrosegregation data.

The typical thermal profile used for our experiments is shown in Fig. 4. The data points represent the imposed thermal profile, as recorded on the outer surface of the quartz ampoules. The temperature profile along the ampoule axis within the sample is represented by the broken line. The central axis of the liquid region of the specimen is slightly cooler (up to 5 K) than the ampoule outside temperature. Whereas the central axis of the solid region of the sample is slightly hotter than the ampoule outer wall. This is expected because in the melt portion the heat flows into

the ampoule from outside and in the solid portion the heat flow is from inside the ampoule towards outside. The thermal gradient measured in the liquid at the solidus temperature was about 34 K cm^{-1}.

Fig. 5 shows a typical view of the liquid-solid interface for the specimen grown in a 2.0 cm diameter ampoule. The heater wires, stationary with respect to the ampoule seen in this figure, were used to accurately measure the interface growth speed, as opposed to the ampoule withdrawal speed. The planar liquid-solid interface was observed to be convex towards the liquid, the extent of convexity varying with the distance solidified. Convexity of the interface is clearly visible in the beginning of solidification (Fig. 5(a), distance solidified ≈0.6 cm). The convexity decreases significantly and the interface becomes reasonably flat after about 1 cm of growth (Fig. 5(b), distance solidified 3.3 cm), and then onwards it retains such a shape for most of the solidification distance. Towards the end it again develops significant convexity towards the liquid (Fig. 5(c), distance solidified ≈6.0 cm).

Fig. 6 shows the change in fluid velocity as a function of distance from the solid-liquid interface for the specimen grown in the 2.0 cm diameter ampoule. The convective speeds were experimentally measured by recording the motion of some dark impurity particles occasionally present in the specimens. The inset in Fig. 6 shows a typical path followed by one such particle, rising into the melt towards the back side of the ampoule and coming down approximately along the central axis of the ampoule, and repeating this cycle again and again. The particle speed, while rising from the interface, decreased from 0.06 cm s^{-1} near the interface to about 0.03 cm s^{-1} at a distance of 1.2 cm from the interface. The particle then moved forward,

towards the ampoule axis, before starting its descent towards the interface. Its downward speed increased from about 0.02 cm s^{-1} to 0.04 cm s^{-1}, before it moved backward, towards the back of the ampoule, and again started its upwards journey. A quiescent melt layer (where there was no convection) of about 0.17 cm thickness was observed at the interface.

MACROSEGREGATION: Fig. 7 shows the effect of ampoule diameter on the axial macrosegregation in directionally solidified CsI-1 wt% TlI. This figure plots the thallium iodide content as a function of the fraction distance solidified (F_s). All the three specimens show extensive macrosegregation. The 1 and 2 cm diameter specimens show the classical macrosegregation behavior expected for a well mixed fluid (Ref. 7). The 0.5 cm diameter sample has a larger scatter, and it appears to show a 'S' type of curve, a behavior expected when the solutal boundary layer thickness δ is of the order of D_l/R (Ref. 9). For our growth conditions the D_l/R value is about 0.25 cm ($D_l \approx 10^{-5} cm^2 s^{-1}$).

Fig. 8 shows the variation in light intensity (output) along the length of the directionally solidified specimen (2.0 cm diameter). With the increasing fraction solid the light output decreases, the decrease being very large near towards the last portion to solidify. The light output is plotted as a function of the thallium iodide content of the alloy in Fig. 9. Higher TlI content results in reduced light output. This figure indicates that the maximum scintillation efficiency possibly occurs at thallium-iodide content of even less than 0.23 wt%. There is therefore a need to investigate this behavior for CsI-TlI alloys containing 0.05 to 0.1 wt% TlI to obtain the most optimum TlI content.

Fig. 10(a) shows the radial macrosegregation as observed by the light output variation in radial direction on three locations along the length of the directionally solidified sample (2.0 cm diameter). Each data point represents an average of four measurements taken at a given radial distance from the center. These measurements would indicate that despite a large axial macrosegregation in this specimen there is little radial macrosegregation.

The spatial resolution of electron microprobe technique is much better (2.0 μm) than the light output measurement method described earlier (0.3 cm). Therefore microprobe analysis was used to obtain a semiquantitative characterization of the radial macrosegregation for the 2.0 cm diameter sample along its length as shown in Fig. 10(b). This figure plots the intensity of the thallium K_α line as a function of the radial distance from the center of the ampoule for four transverse sections. The fraction solid values corresponding to the transverse sections are indicated in this figure. The liquid-solid interface morphologies corresponding to these fraction solid were shown in Fig. 5. This figure shows the above described axial macrosegregation, increase in thallium content with the fraction distance solidified (F_s). This figure shows that there is a tendency for solute build up as one moves towards the outer periphery of the specimen cross-section. The radial macrosegregation is quite small for most of the specimen length, F_s=0.14, 0.35 and 0.50, (Fig. 5(a)). However, towards the end of solidification (F_s=0.85) when the thallium content of the melt is large and the liquid-solid interface is convex towards the liquid (Fig. 5(c)) considerable radial macrosegregation is observed, thallium content increasing radially from the center towards the outer surface.

DISCUSSION

RADIAL MACROSEGREGATION: The solutal profile in the melt ahead of the liquid-solid interface during plane front directional solidification of CsI-1wt% TlI alloy, with melt on top and solid below with gravity pointing down), is expected to be stable against natural convection (density of TlI, 7.29 gcm^{-3}, is larger than CsI, 4.51 gcm^{-3}). However, the radial thermal gradient in the melt (liquid along the ampoule axis was up to 5K cooler than the ampoule outer wall, Fig. 4) is expected to cause convection ahead of the liquid-solid interface. The convection currents would be composed of the warmer liquid rising along the outer periphery and the cooler liquid coming down towards the interface along the ampoule axis. This is in agreement with the experimentally observed fluid flow behavior (Fig. 6). Such a fluid flow pattern will be expected to transport solute near the liquid-solid interface from the central axis of the crystal towards its outer periphery. This will result in an interface shape which is convex towards the melt (solute rich outer periphery will have a lower melting point), as is observed (Fig. 5). It will also produce the observed radial macrosegregation, thallium content increasing radially from the center towards the outer surface (Fig. 10(b)).

AXIAL MACROSEGREGATION: We will examine the axial macrosegregation behavior in our samples in terms of the solutal boundary layer model of Favier (Refs.8,9). According to this analysis, the solute content during the initial transient (as a function of distance (x)) in the presence of convection is given as,

$$C_s(x)/C_o = k(\Delta)\{1 - A_1(\Delta)\exp(-\beta_1 Rx/4D_l)\}$$

where,

$A_1(\Delta)=[8(1-k_o)[k_o+(1-k_o)\exp(-\Delta)]\sin^2\alpha_1]/(\beta_1\Delta[1-2\cos^2\alpha_1/[\Delta(1-2k_o)])$

and $\beta= 1+(1-2k_o)^2\ \mathrm{Tan}^2(\alpha_1)$

and α_1 is solution of the following equation,

$2\alpha_1\cos\alpha_1-(1-2k_o)\ \Delta\ \sin(\alpha_1)=0$

if $(2k_o-1)\Delta/2 < -1$, then $\beta=1-(1-2k_o)^2\ \mathrm{Tanh}^2(\alpha_1)$.

Favier gives the following relationship as a function of distance from the location where the initial transient region is finished (x^*) for a total length of L.

$C_s(x)/C_o=C_s(x^*)+ [k(\Delta)/[1-k(\Delta)]] * [1-C_s(x^*)]^*[[(L-x)/(L-x^*)]^{[k(\Delta)-1]}-1]$

where $\Delta=R\delta/D_l$ is the parameter of Burton, Prim and Slichter.

Fig. 11 shows the experimentally observed macrosegregation behavior for the samples solidified in three different diameter ampoules. Because of their varying specimen lengths the data for the three diameters, 0.5, 1.0 and 2.0 cm, are plotted separately in Fig. 11. The curves correspond to the predicted behavior from the above model for various Δ values. A diffusion coefficient (D_l) value of $1.05X10^{-5}$ cm^2s^{-1} has been used in obtaining these plots. As indicated by Favier (Refs. 8,9) the shape of the macrosegregation profile is concave upwards for small Δ values (0.5 to 1.0). For the larger Δ values of (2 to 4) the macrosegregation profiles has a 'S' type of shape. The experimental data for the 0.5 cm diameter (Fig. 11(a)) appear to show a tendency for the 'S' type of behavior. The 1.0 (Fig. 11(b)) and 2.0 cm (Fig. 11(c)) diameter specimens clearly show the 'concave upwards' profiles expected for the small Δ values associated with more intense convection. These plots show the expected increase in the intensity of convection with increase in ampoule diameter. The 1.0 cm diameter specimen shows the best fit to a Δ value between 1 and 2; whereas the 2.0

cm diameter specimen shows the best fit to a Δ value of about 0.5. The Δ value of 0.5 corresponds to a solutal boundary layer (δ) of about 0.13 cm. This is in a good agreement with the boundary layer thickness observed experimentally (zone of no observable fluid motion next to the interface, Fig. 6) about 0.17 cm.

CONCLUSIONS

Convection during plane front directional solidification of a transparent CsI-1 wt% TlI alloy has been examined in this study and correlated with the resulting radial and axial macrosegregation. Following conclusions can be drawn from this investigation.

(1) Radial thermal gradients cause extensive convection in the melt despite the expected stabilizing influence of the TlI rich solutal boundary layer ahead of the liquid-solid interface. (2) Decreasing the ampoule diameter reduces the convection. However, it is not elminated even for the smallest diameter of 0.5 cm examined in this study.

(3) Axial macrosegregation along the growth direction of the directionally solidified crystals is in reasonable agreement with the behavior predicted from the solutal boundary layer model of Favier (Refs. 8,9).

(4) Scintillation efficiency of CsI crystals, as indicated by their light output, decreases with increasing thallium iodide content (0.23 to 1.82 wt% TlI). Lower TlI content alloys should be examined for determining the optimum dopant content.

ACKNOWLEDGEMENTS

This research was supported by a grant (NCC-3-96) from NASA-Lewis Research Center, Cleveland, Ohio 44135. Appreciation is expressed to Bruce Rosenthal and Dr.

M.R. Farukhi for their help, and to Thomas K. Glasgow for many helpful discussions.

REFERENCES

1. V.G. Smith, W.A. Tiller and J.W. Rutter, Canadian J. Phys., vol. 33, (1955), 725.

2. W.A. Tiller, K.A. Jackson. J.W. Rutter and B. Chalmers, Acta Metall., vol. 1, (1953), 419.

3. C.E. Chang and W.R. Wilcox, J. Crystal Growth, vol. 21, (1974), 135.

4. T. Jasinski and W.M. Rohsenow, J. Crystal Growth, vol. 61, (1983), 39.

5. P.M. Adornato and R.A. Brown, J. Crystal Growth, vol. 80, (1987), 155.

6. C.J. Chang and R.A. Brown, J. Crystal Growth, vol. 63, (1983), 343.

7. J.A. Burton, R.C. Prim and W.P. Slichter, J. Chem. Phys., vol. 21, (1953), 1987.

8. J.J. Favier, Acta Metall., vol. 29, (1981), 197.

9. J.J. Favier, Acta Metall., vol. 29, (1981), 205.

10. J.J. Favier, J. Cryst. Growth, vol.99 (1990), 18.

11. A. Schiraldi, E. Pezzati and P. Rossi, Zeitschrift fur Physikalishe Chemie Neue Folge, Bd. 121, (1980), 17.

12. M.R. Farukhi, "Scintillation Detectors for CT Applications, Workshop on Transmission and Emission Computed Tomography", Seoul, Korea (1978).

13. B.C. Grabmaier, IEEE Trans. Nuclear Sci., vol. NS-31, No. 1, (1984), 372.

14. B.K. Utts and S.E. Spagno, IEEE Trans. Nucl. Sci., vol. 37, No. 2, Pt.1, (1990), 134.

15. Handbbok of Chem. and Physics, 51st edition, 1970-71, P.B-82.

LIST OF FIGURES

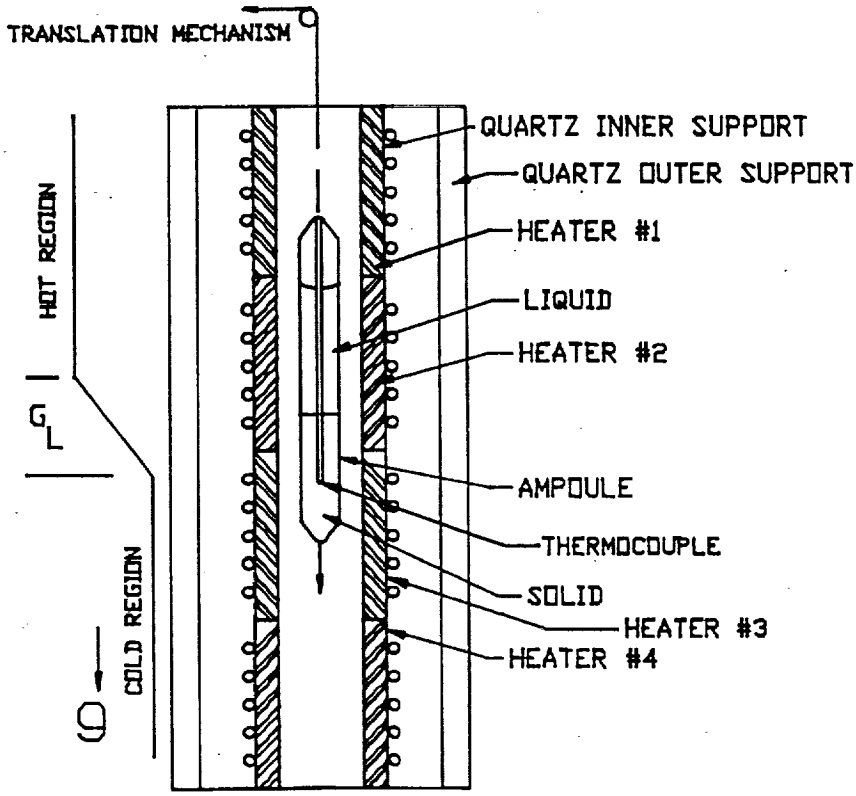

1. A schematic view of the transparent directional solidification furnace and the ampoule.

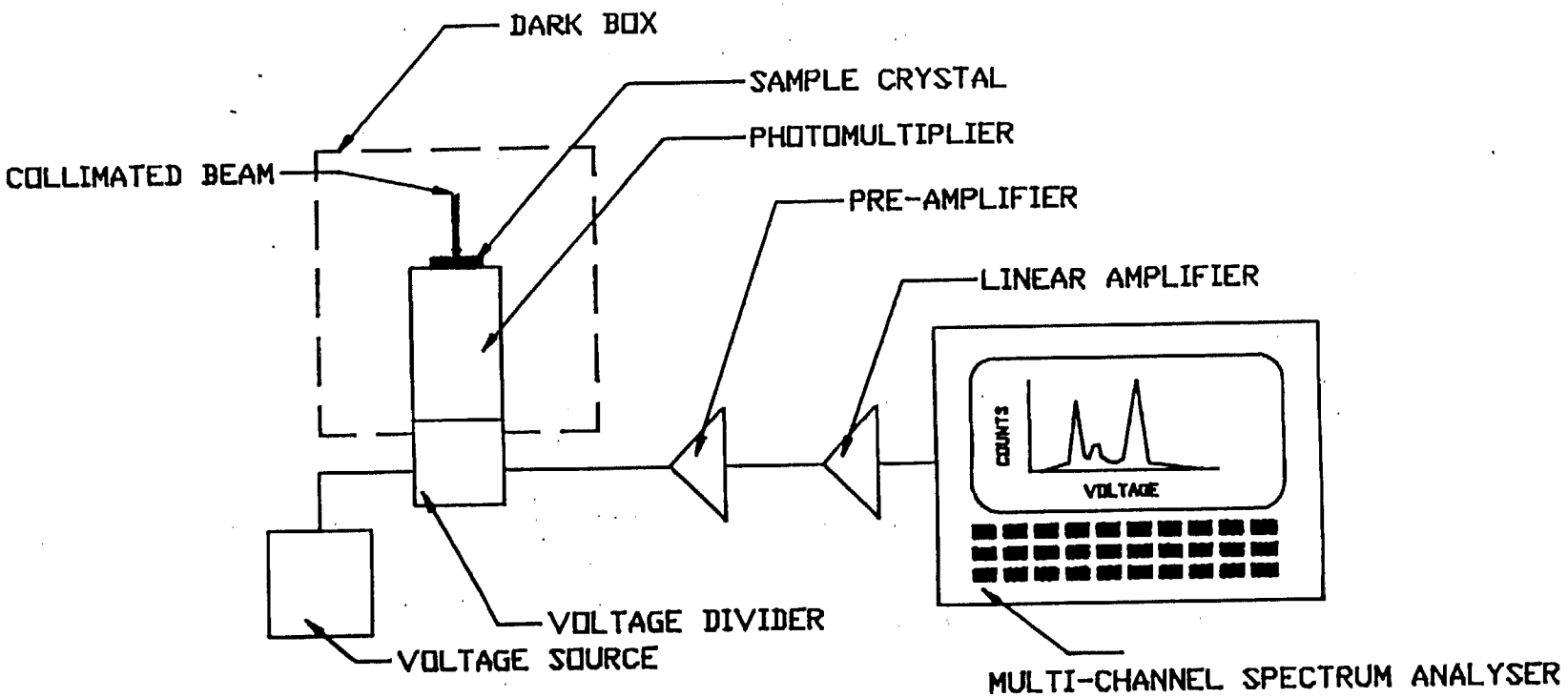

2. Experimental assembly for measuring the scintillation efficiency (intensity of output light) in CsI-Tl alloys.

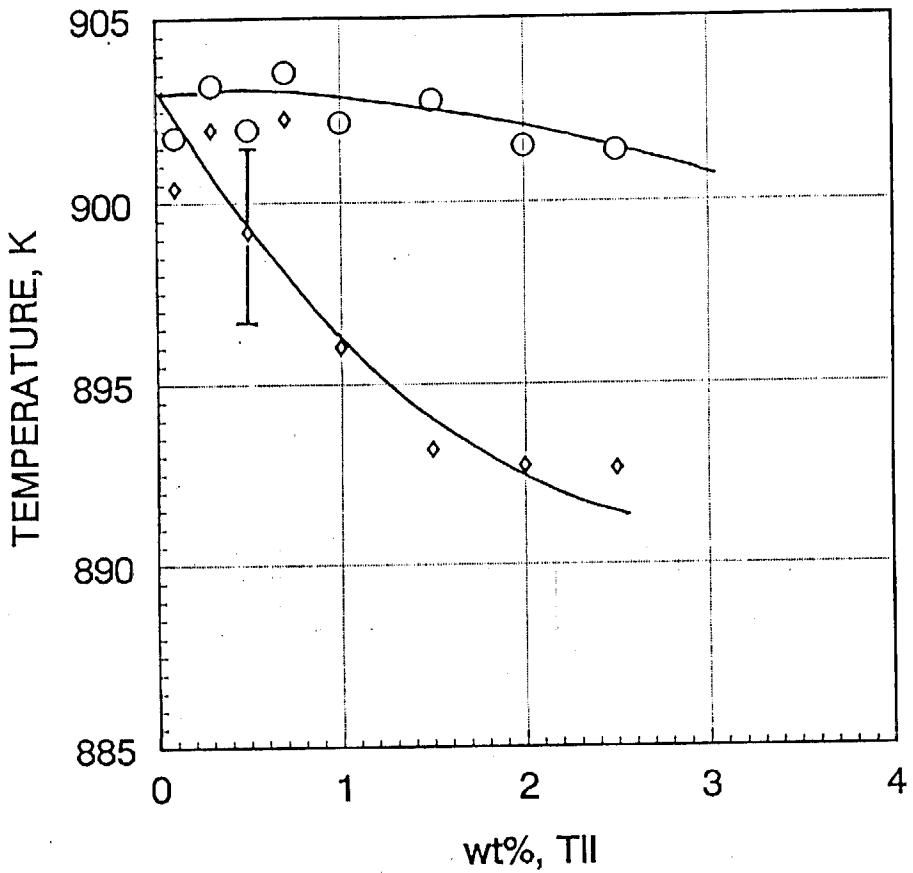

3. The CsI-TlI phase diagram as determined in this work.

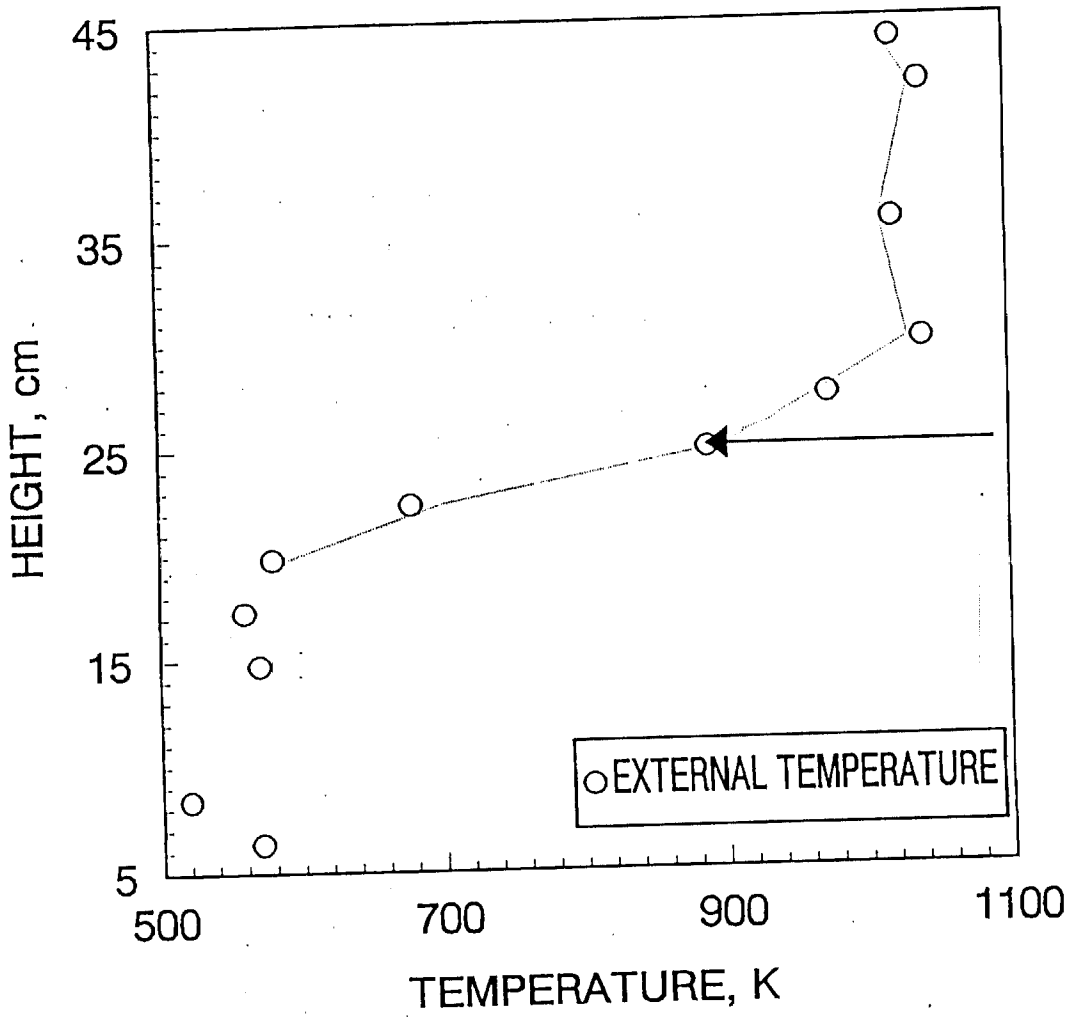

4. Thermal profiles used during directional solidification. The symbols represent the imposed thermal profile (as measured on the outside wall of the crucible) and the solid line represents the temperature inside the sample, along its axis.

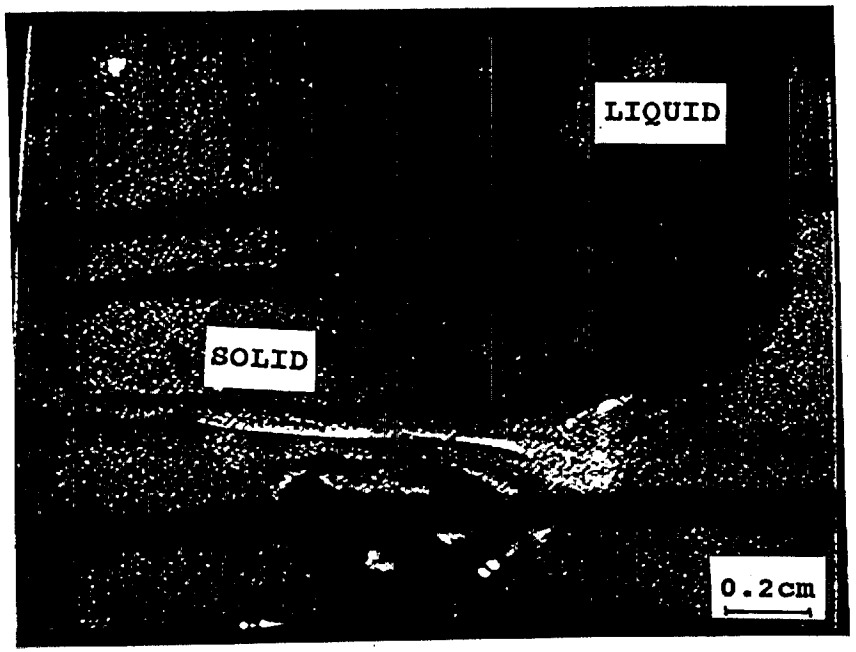

(a)

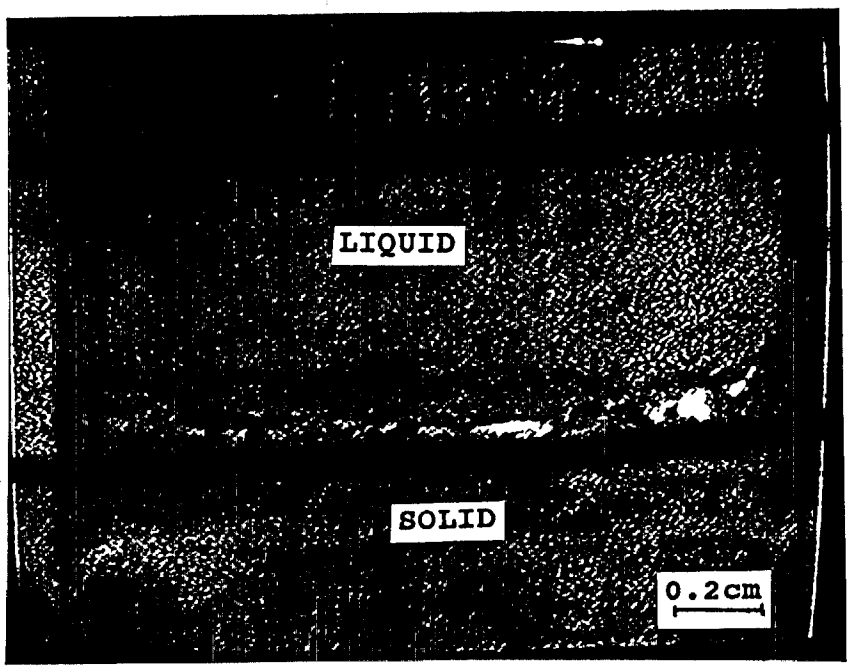

(b)

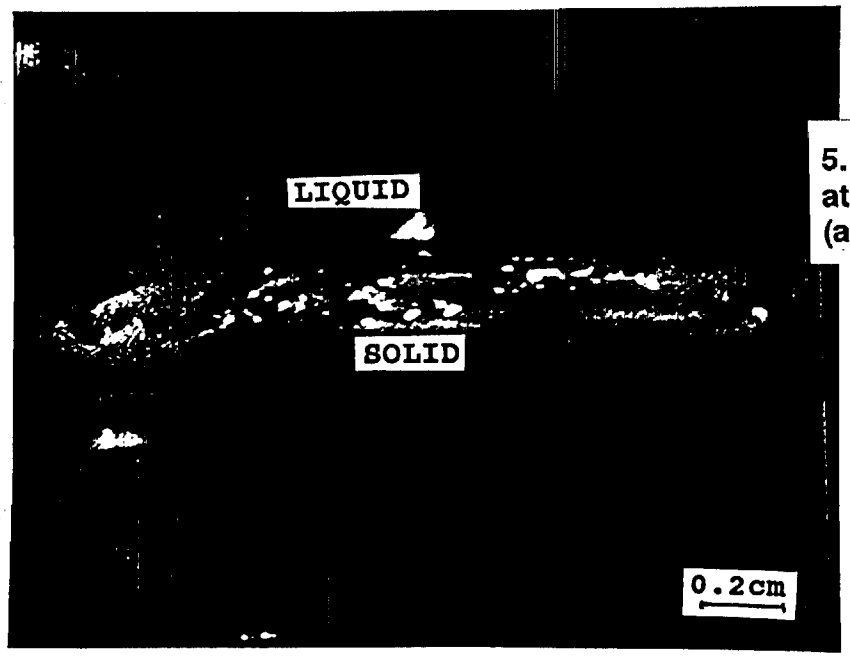

(c)

5. Typical views of the liquid-solid interface for the 2.0 cm diameter sample grow at 0.4 μms^{-1} with a thermal gradient of 34 kcm^{-1} at various solidification distances. (a) 0.6 cm, (b) 3.3 cm, and (c) 6.0 cm.

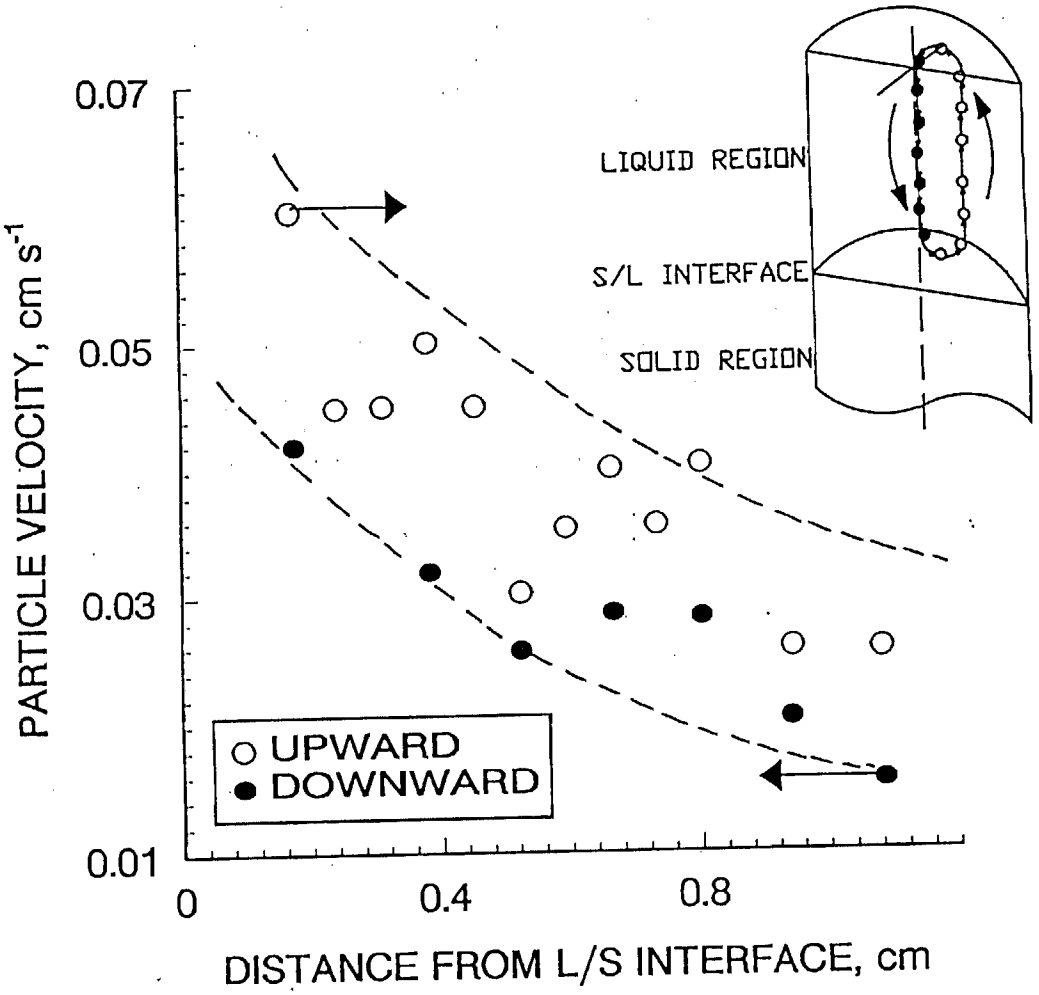

6. Fluid velocity as a function of distance from the interface, the upward and downward velocities are indicated by open and filled symbols. The inset shows one typical current as observed by motion of small impurity particle for a 2 cm diameter specimen growing at 0.4 μms^{-1} with a thermal gradient of 34 kcm^{-1}.

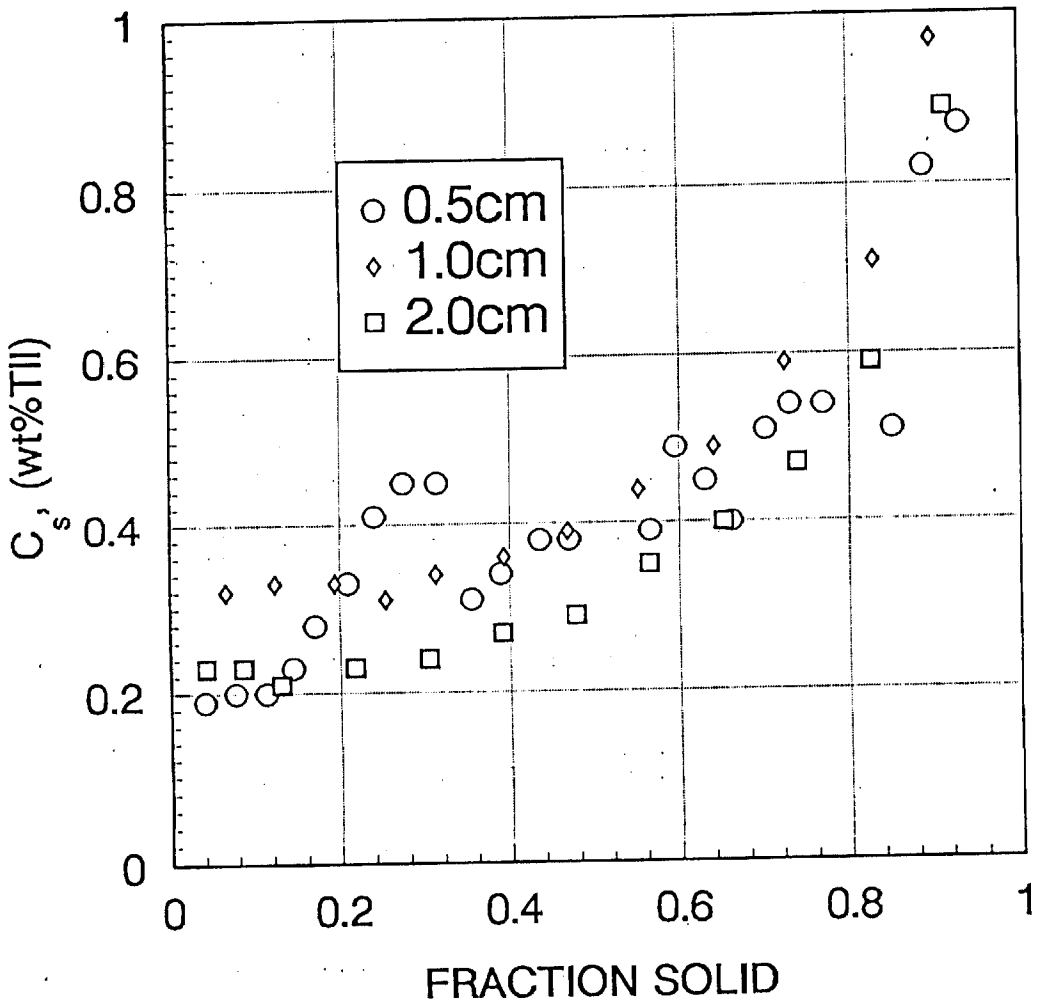

7. Macrosegregation along the length of directionally solidified CsI-1 wt% TlI alloy as a function of the ampoule diameter (G_l=34K cm^{-1} and R=0.4 μm s^{-1}), 0.5, 1.0, and 2.0 cm.

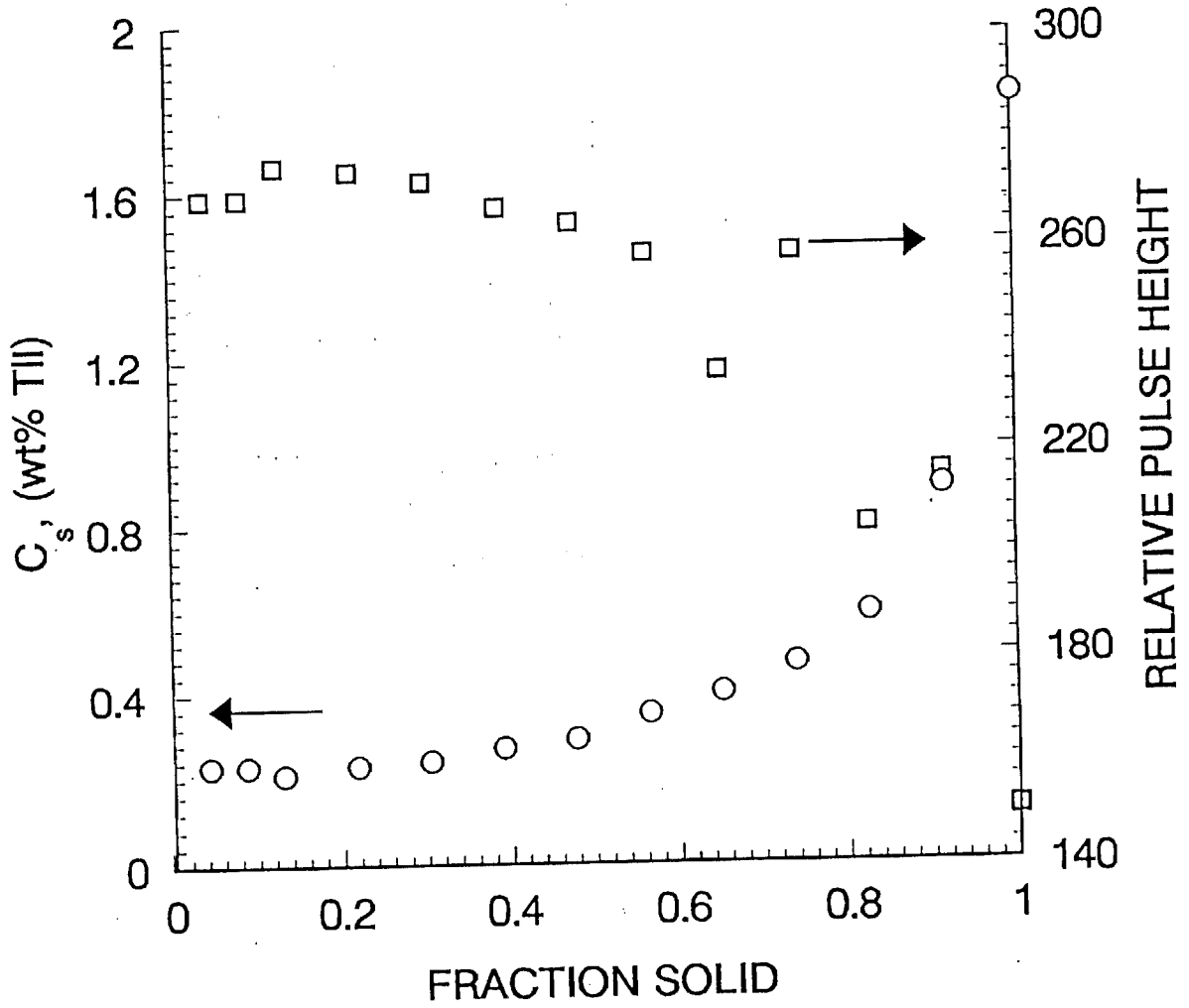

8. Variation in scintillation light output along the length of the directionally solidified CsI-1wt%TlI specimen (34 K cm^{-1}, 0.4 $\mu m\ s^{-1}$, crucible diameter=2.0 cm).

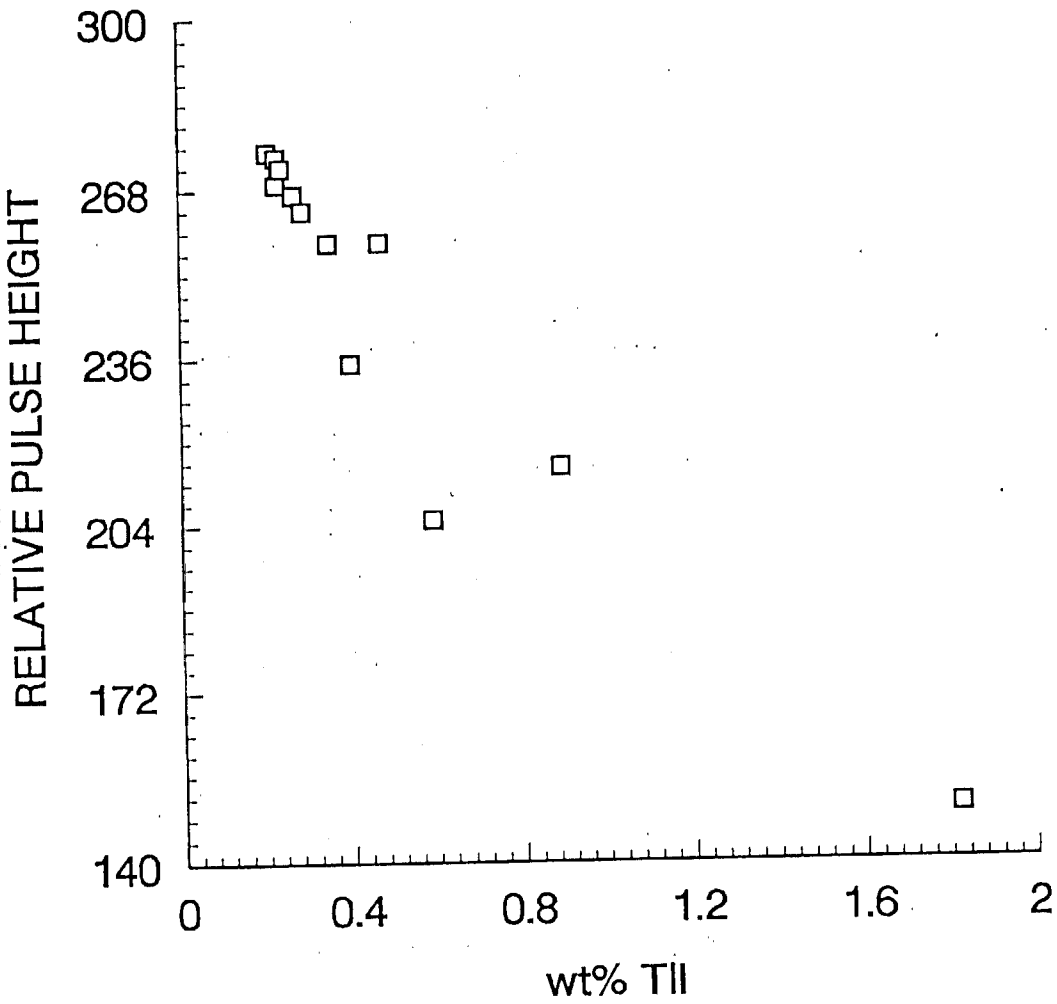

9. Dependence of the scintillation efficiency (intensity of output light) on the thallium iodide content of CsI alloy.

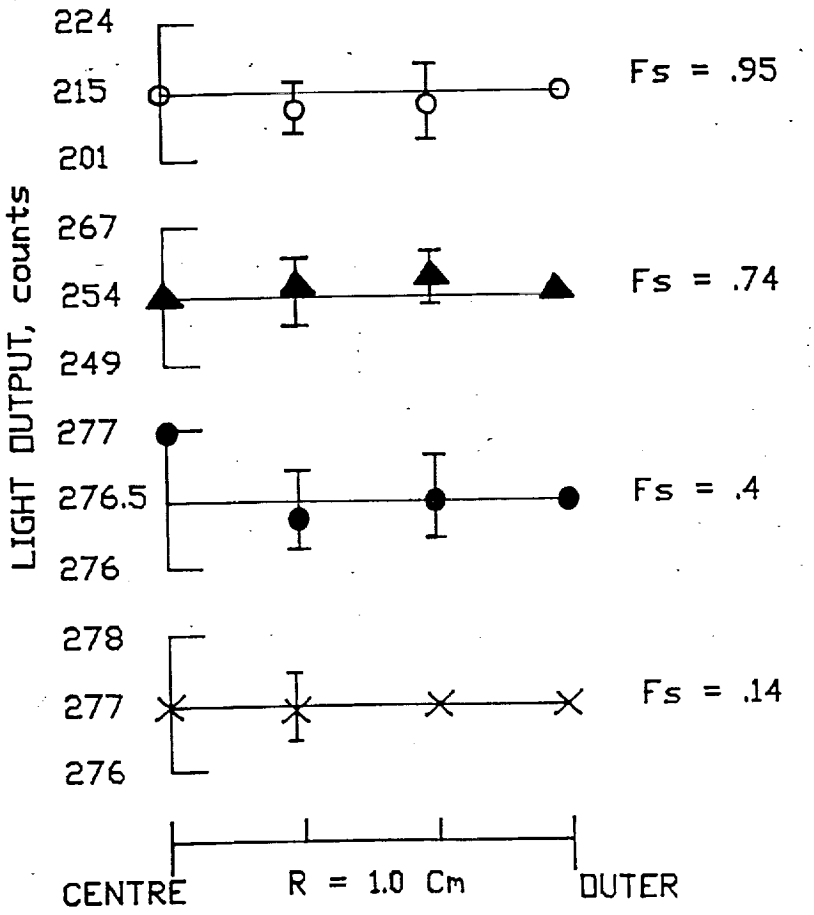

10. Radial macrosegregation on transverse slices cut at three locations along the directionally solidified length (ampoule diameter=2 cm). The corresponding fraction solidified is indicated in these figures.

(a) The scintillation light distributions.

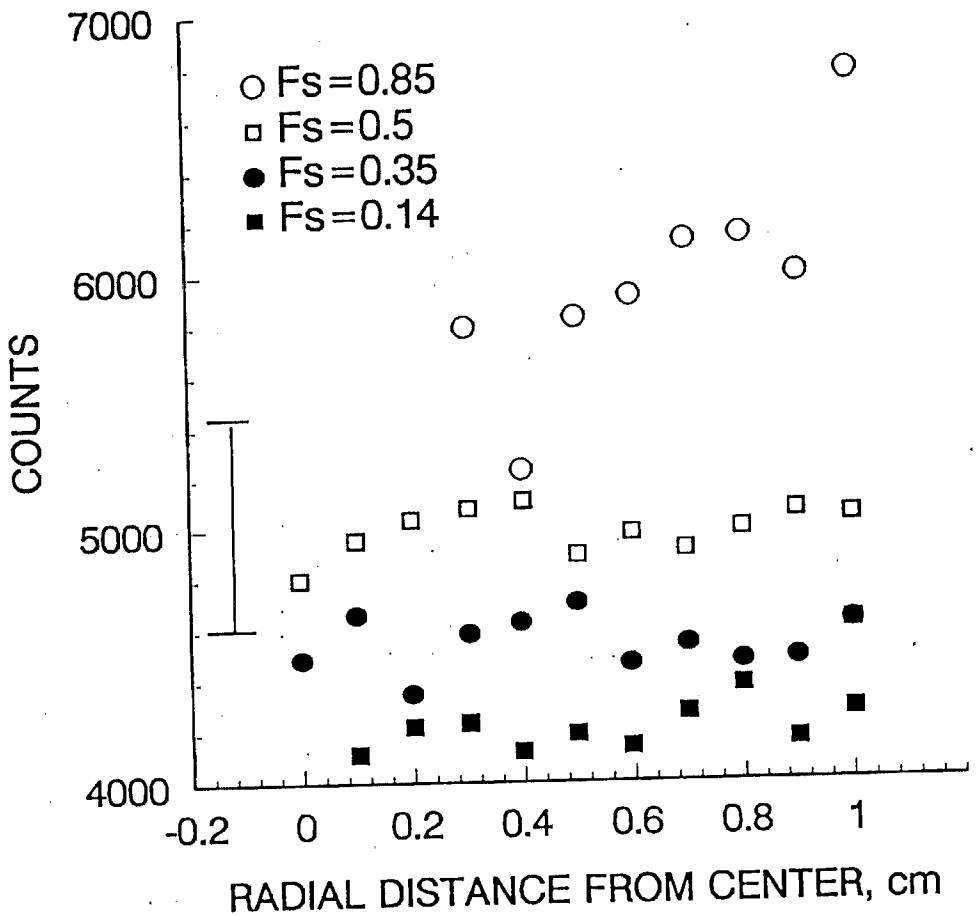

10 (b) Electron microprobe analysis of thallium.

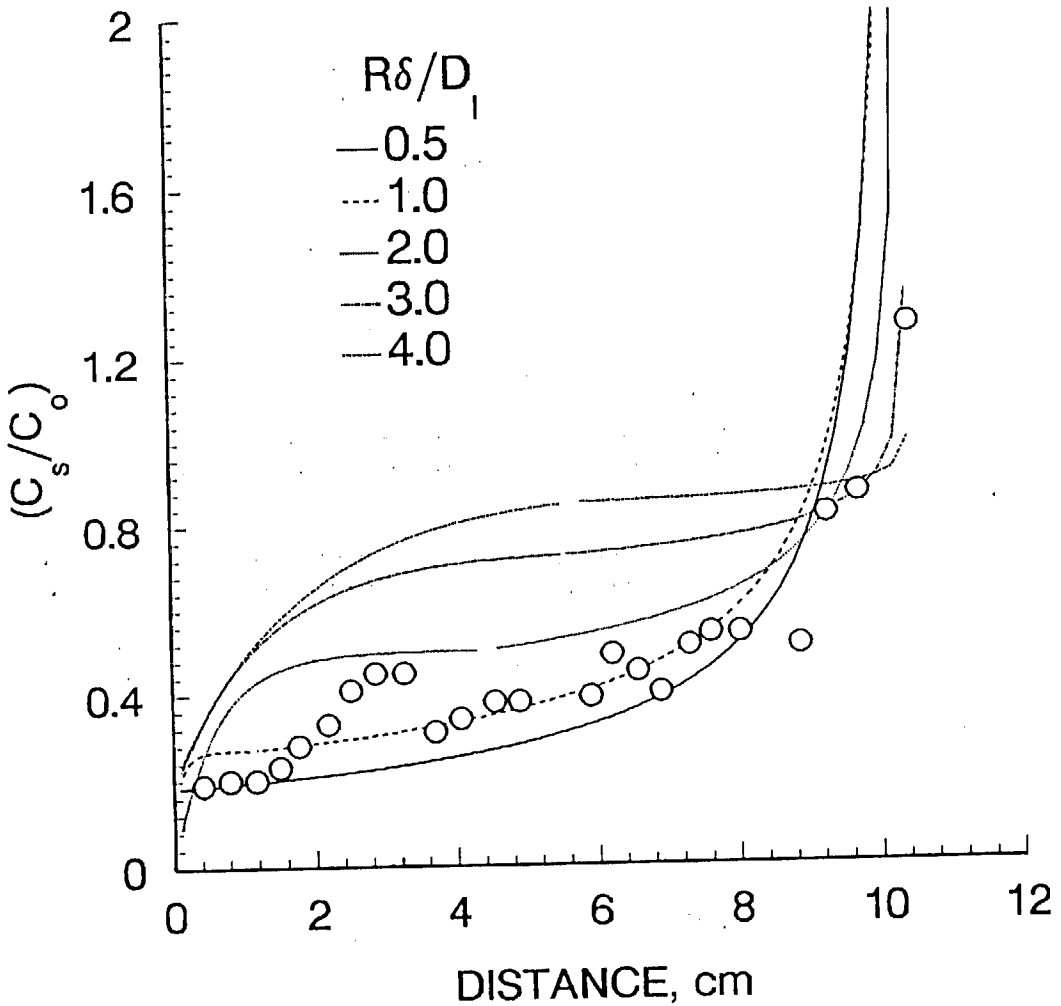

11. Comparison of the experimentally observed macrosegregation with predictions from the solutal boundary layer model of Favier (Ref. 8).
(a) 0.5 cm diameter ampoule

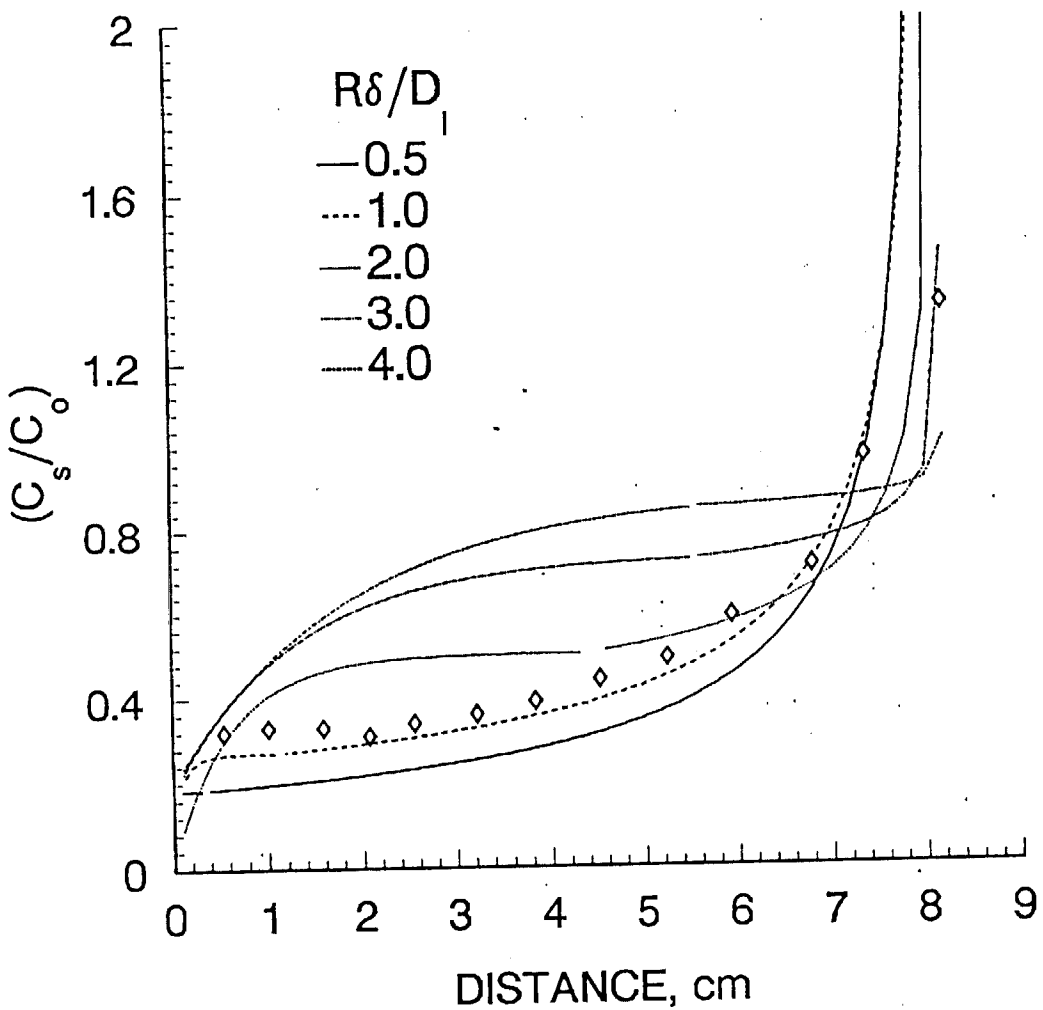

11 (b) 1.0 cm diameter ampoule

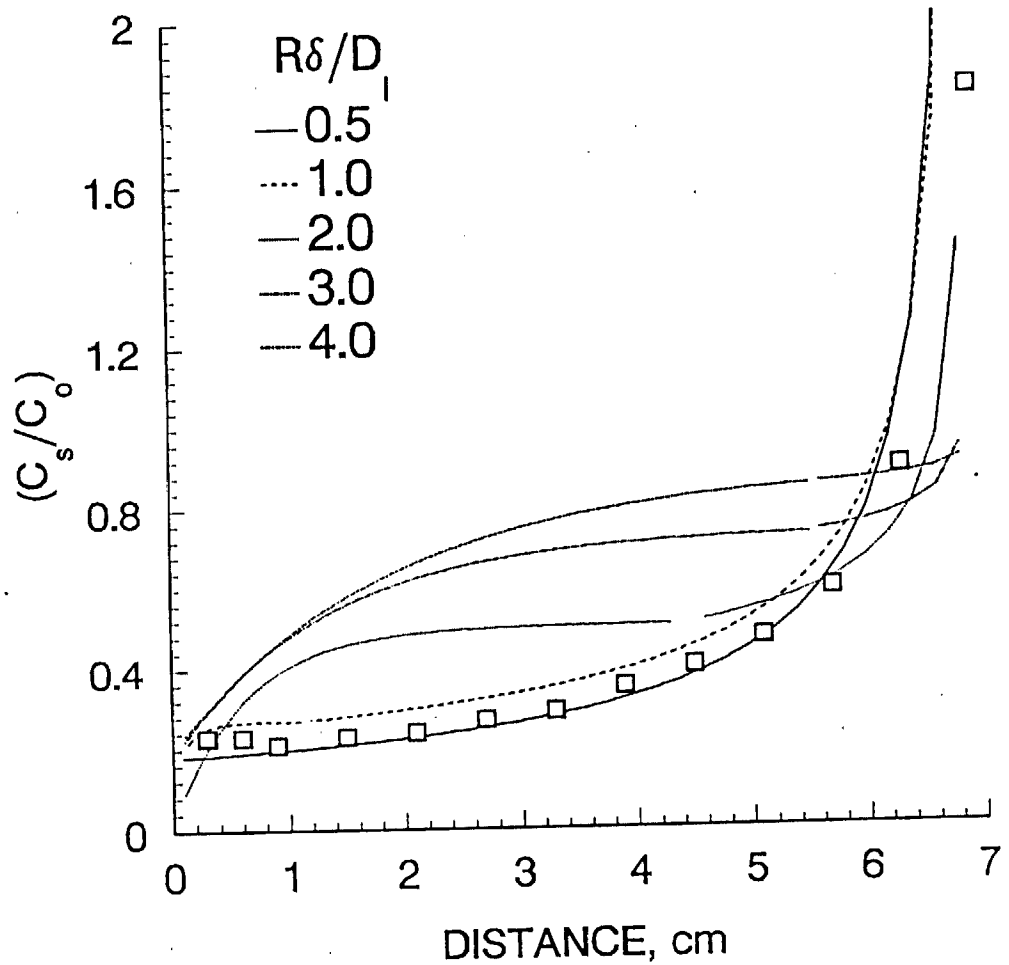

11 (c) 2.0 cm diameter ampoule